

Effect of Water Molecules on Crystallization During Uniaxial Drawing of Poly(ethylene terephthalate) Films

E. DARGENT, G. DENIS, C. CARON, J. M. SAITER, J. GRENET

Laboratoire d'Etude et de Caractérisation des Amorphes et des Polymères, Université de Rouen, Faculté des Sciences, 76821 Mont-Saint-Aignan Cedex

Received 12 July 1999; accepted 23 October 1999

ABSTRACT: The role played by sorbed water molecules present within poly(ethylene terephthalate) film at the moment of uniaxial drawing on the appearance and the percentage of the strain-induced crystalline (SIC) phase is investigated by birefringence, X-ray diffraction, and differential scanning calorimetry measurements. We show that, for low draw ratio, water plays its traditional plasticizer effects. The SIC phase appears for a draw ratio, which depends weakly on the relative humidity. The water does not modify the degree of crystallinity of drawn films but impedes the growth of a part of the crystallites and modifies their crystalline size. For high draw ratio, water impedes the orientation of the amorphous phase. © 2000 John Wiley & Sons, Inc. *J Appl Polym Sci* 77: 1056–1066, 2000

Key words: poly(ethylene terephthalate); water content; differential scanning calorimetry; birefringence; strain-induced crystallization

INTRODUCTION

Poly(ethylene terephthalate) (PET) is included in the group of hydrophobic polymers in regard to the small amount of water that it can absorb under saturation conditions,¹ but it can also be considered as hygroscopic thermoplastic, which absorbs moisture from its environment at a relatively rapid rate.² In spite of this hydrophobic character, its physical properties are considerably affected by such small amount of absorbed water and, as a consequence, serious problems can appear in industrial applications by altering the dimensional stability of manufactured articles, for example. In packaging industries, PET is commonly used to manufacture water or soft drink bottles and so it is often in the presence of water. This is one of the reasons for which this material and the role of water on its properties are inten-

sively studied. From a more academic point of view, PET is also a very good candidate for fundamental studies. Indeed, depending on the thermal cycles performed, it is possible and easy to obtain a wholly amorphous or a partially crystallized materials from controlled experimental ways. Moreover, this semicrystalline state can be reached directly from the liquid state by cooling with a low cooling rate in order to allow nucleation and crystal growth, from the vitreous state by heating above the glass transition temperature (cold thermal crystallization), and also by drawing up to a critical draw ratio (strain-induced crystallization).

For a wholly amorphous film, the effects of sorbed water molecules lead to a shift of $\approx 15^\circ\text{C}$ toward lower temperatures of the glass transition temperature (T_g) with increasing the relative humidity (rh) from $rh = 0$ (dry sample) to $rh = 100\%$ (under saturation condition).³ This variation of the glass transition temperature is associated to a plasticization effect. The presence of plasticizer in the polymer decreases the inter-

Correspondence to: E. Dargent.

Journal of Applied Polymer Science, Vol. 77, 1056–1066 (2000)
© 2000 John Wiley & Sons, Inc.

chain interactions and, at the limit, can lead to a suppression of the cooperative motion of the segments, which are involved in the glass transition phenomenon.⁴ This plasticization effect also modifies the relaxation kinetics that occur at a temperature $T_a < T_g$ (called the annealing temperature) by decreasing the apparent activation energy for the relaxation time by 30%.⁵ In the field of barrier behavior, water vapor diffusion through uniaxially⁶ and biaxially⁷ oriented PET films have been investigated. It was shown that the alignment of the benzene ring component of the molecular chain along the draw direction for an uniaxially oriented film; also, the orientation of the plane of the same benzene rings parallel to the sample surface, a phenomenon enhanced for a biaxially oriented film, leads to a decrease in the permeability of the films.

At high moisture content, isothermal crystallization of PET from the glassy state has shown an increase of the overall rate of crystallization primarily due to an increase of the nucleation rate while the spherulite growth rate appeared to be independent of the moisture content.⁸ The same phenomenon was observed on an amorphous film with a concomitant decrease of the cold crystallization temperature T_c (from 128 to 119°C).³ The structural changes in semicrystalline PET induced by annealing under dry and wet conditions were also investigated using X-ray diffraction (XRD), density, and differential scanning calorimetry (DSC) measurements.⁹ It was concluded that the increase in lamellar thickness and crystal size was larger for the wet PET than for the dry one.

Absorbed moisture can cause also significant effects on the chemical stability of PET. The possibility of hydrolysis reactions was mentioned during a prolonged storage at high humidity and high temperatures.¹⁰ This problem is crucial for transforming pellets to manufactured products and is generally solved by drying PET pellets above T_g . After this transformation process, a semifinished product (injected preforms, extruded films) is often obtained. A second transformation process bringing into play a drawing period could occur to get the final commercial product (blowed bottles, uni- or biaxially drawn films). In this field, it is now established that a strain-induced crystalline (SIC) phase and that a fiber texture appear during uniaxial deformation of dry PET above a critical value for the draw ratio.^{11,12} In this work, the role plays by sorbed water molecules present in PET film at the moment of uniaxial drawing on the apparition of the SIC phase,

on the degree of crystallinity, and on the crystalline phase structure is investigated by means of birefringence, XRD and DSC measurements.

EXPERIMENTAL

Drawn samples of PET films were prepared from 0.5-mm-thick PET sheets with a number-average molecular weight $\overline{M}_n = 31,000 \text{ g mol}^{-1}$ and a weight-average molecular weight $\overline{M}_w = 62,000 \text{ g mol}^{-1}$. Experimental measurements were performed on isotropic and amorphous PET sheets, judging from birefringence, density, and XRD measurements. Dry PET films were obtained after drying at room temperature in a vacuum desiccator in the presence of P_2O_5 until a constant weight was obtained (during 5 days). Wet films were achieved by immersion in water at room temperature until a constant weight was obtained (during 15 days).

Before the drawing period, the films were placed in the heating chamber of a tensile machine at 95°C during 5 min to allow an homogeneous temperature distribution in the films. The sample temperature were controlled by an optical pyrometer. The dry films were annealed in the presence of desiccated air and no water absorption was observed during annealing while the wet films were annealed in the presence of a water-vapor-saturated atmosphere. Nevertheless, for the latter samples, a decrease of the water content is observed for these films during the preheating period. By this procedure, the relative humidity of the matter decreases from $rh = 100\%$ to $rh = 76\%$ at the beginning of the drawing experiments. Then, the films ($40 \times 60 \text{ mm}$) were uniaxially drawn at a strain rate of 0.14 s^{-1} in the tensile machine. The drawing temperature (95°C) was chosen between the glass transition temperature and the cold crystallization temperature to allow homogeneous drawing and to avoid thermal crystallization. After drawing, the material; is cold-air-quenched to room temperature in order to freeze in its structural state. Finally, different samples are cut from the drawn materials and the draw ratio λ , equal to the ratio of the extended length over the original length, is measured. It was found that λ varied from 1 to 7.2.

To analyze the effects of water molecules on the crystallization induced by the drawing, we used birefringence, wide-angle X-ray scattering (WAXS), and DSC analysis. However, because it is well

known that the presence of sorbed water modify the DSC responses of the material,³ we have to desorb the remaining water before any DSC analysis. So, the wet- and dry-drawn samples were stored in the vacuum desiccator during 5 days before analysis. By this treatment, we have checked that the relative humidity of the wet drawn samples decreased from to 0.0% *rh*, whatever the draw ratio, while the dry-drawn samples remained dry. By this way, the only effect of water on strain-induced crystallization could be investigated.

Optical anisotropy of samples was measured by birefringence measurements at room temperature and using a spectrophotometric method.¹³ Wide-angle X-ray diffraction (WAXD) was performed in reflection using a SIEMENS D5000 goniometer, worked at 40 kV and 30 mA, using Fe-filtered Co- K_{α} radiation ($\lambda^* = 0.1789$ nm). The reflection procedure was used to obtain the scattered intensity versus 2θ , where θ is the angle between the incident beam and a reference axe parallel to the surface of the sample. Calorimetric investigations were performed with a Perkin-Elmer DSC7 calorimeter. Its calibration in temperature and energy was achieved at 10 K min^{-1} under nitrogen atmosphere using indium as a standard. The crystallization temperature T_c is determined from the minimum of the crystallization peak. The glass transition temperature T_g is the onset temperature of the glass transition, while the melting temperature is determined at the maximum of the main fusion peak. All the DSC curves presented in the following are normalized to 1 mg.

RESULTS

Birefringence

Birefringence is due to a difference between the principal refractive indices within a material, and its variations can be interpreted in regard to average orientation of the macromolecules. The birefringence data are displayed in Figure 1, and the dashed lines are solely included to facilitate visualization of changes over the draw ratio (λ). For the dry-drawn samples, the variations of the birefringence Δn with λ exhibit several distinct stages. First, for λ values up to ≈ 2 , Δn increases from $\Delta n = 1.10^{-3}$ to $\Delta n \approx 5 \cdot 10^{-2}$. For $\lambda \approx 2$, a distinctive discontinuity occurs, and the birefringence drastically changes from $\Delta n \approx 5 \cdot 10^{-2}$

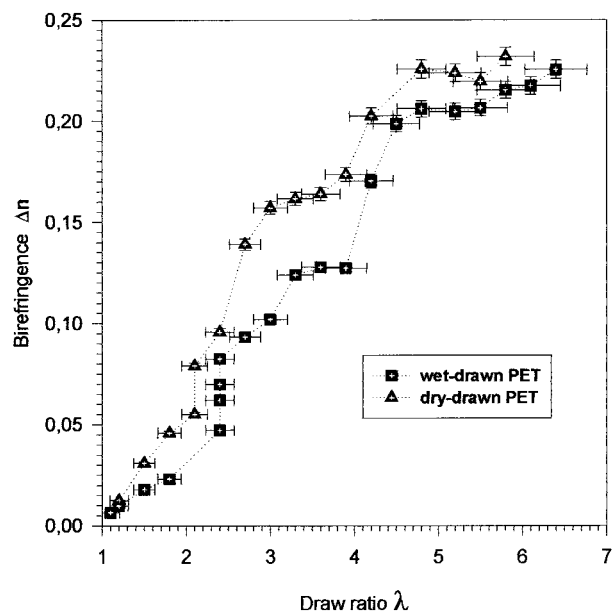


Figure 1 Birefringence versus draw ratio for the dry and the wet samples. Dashed lines are drawn as guides for the eyes.

to $\Delta n \approx 8 \cdot 10^{-2}$. This critical value $\lambda_{c1} \approx 2$ was already observed by F. Rietsch¹⁴ on a PET with a specific viscosity $[\eta] = 0.58$. The birefringence increases for $\lambda \geq 2$ up to 0.16 for $\lambda = 3$, and this value remains practically constant up to $\lambda = 4$. For $\lambda = 4$, a second distinctive discontinuity occurs. This second critical value called λ_{c2} was also observed by F. Rietsch¹⁴ but depends on the PET specific viscosity ($\lambda_{c2} \approx 3$ for $[\eta] = 0.85$, $\lambda_{c2} \approx 4$ for $[\eta] = 0.61$). After this transition, Δn increases to reach a value $\Delta n \approx 0.225$, which will remain constant as far as the rupture of the sample ($\lambda \approx 7$).

The similar sequences are observed for the wet-drawn samples (second set of data points reported in Figure 1). We notice a weak shift of λ_{c1} towards higher draw ratio values leading for the first step to $\lambda_{c1} \approx 2.4$. The intermediate plateau is clearly weaker (0.13), while the final transition and plateau remain unchanged. Finally, for a given draw ratio, the values of Δn observed for a dry-drawn sample are always higher than the values of Δn obtained with a wet-drawn sample.

Calorimetry

For each draw ratio investigated in this work and for dry-drawn and wet-drawn samples, the DSC curves are presented in Figures 2 and 3, respectively. The curve of an undrawn sample (Fig. 3; λ

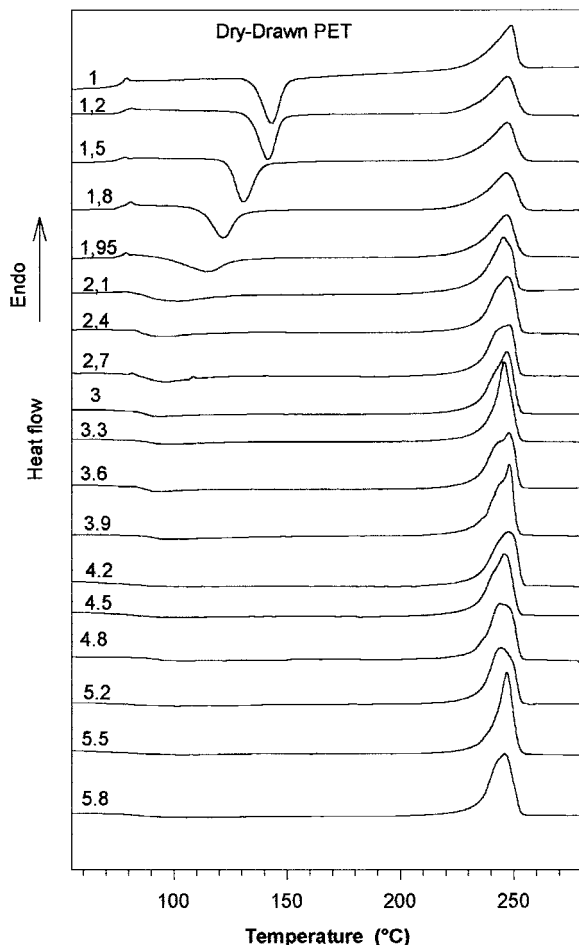


Figure 2 DSC normalized curves for wet samples drawn at various draw ratio (indicated on the figure). The curves are shifted on the heat flow axis for legibility.

= 1) is a standard DSC curve expected for an amorphous PET. It shows (1) the glass transition at $70^{\circ}\text{C} < T_g < 80^{\circ}\text{C}$, evidenced by the endothermic step; (2) the thermal cold crystallization, which is observed by the exothermic peak at $130^{\circ}\text{C} < T_c < 170^{\circ}\text{C}$; and (3) the melting peak of the crystalline phase between 220 and 260°C , which occur as an endothermic peak.

Whatever the drawing process, the glass transition, the cold crystallization, and the melting peaks are practically the same for a given λ value lying between 1 and 2. On the other hand, increasing the draw ratio leads to decrease the cold crystallization temperature toward the glass transition one with a concomitant decreasing of the crystallization enthalpy.

For $2 < \lambda < 4$, which is to say for $\lambda_{c1} < \lambda < \lambda_{c2}$, and whatever the materials, the variations of Cpl

– Cpg (the difference between the thermal capacity in the liquid-like and glassy states at $T = T_g$) decrease continuously, and this difference vanishes when draw ratio reaches λ_{c2} . For the same domain of draw ratio, and for the dry-drawn sample, the variations observed previously for the enthalpy of cold crystallization are carried on, while the value $T_c = 96^{\circ}\text{C}$ remains unchanged. For the wet-drawn sample, the same observations can be done for the values of the enthalpy of cold crystallization; but for the cold crystallization temperature, we observe an increase of its value from $T_c(\lambda_{c1}) = 100^{\circ}\text{C}$ to $T_c(\lambda_{c2}) = 120^{\circ}\text{C}$. The shape of the cold crystallization peak also changes. It appears wider compared with the un-

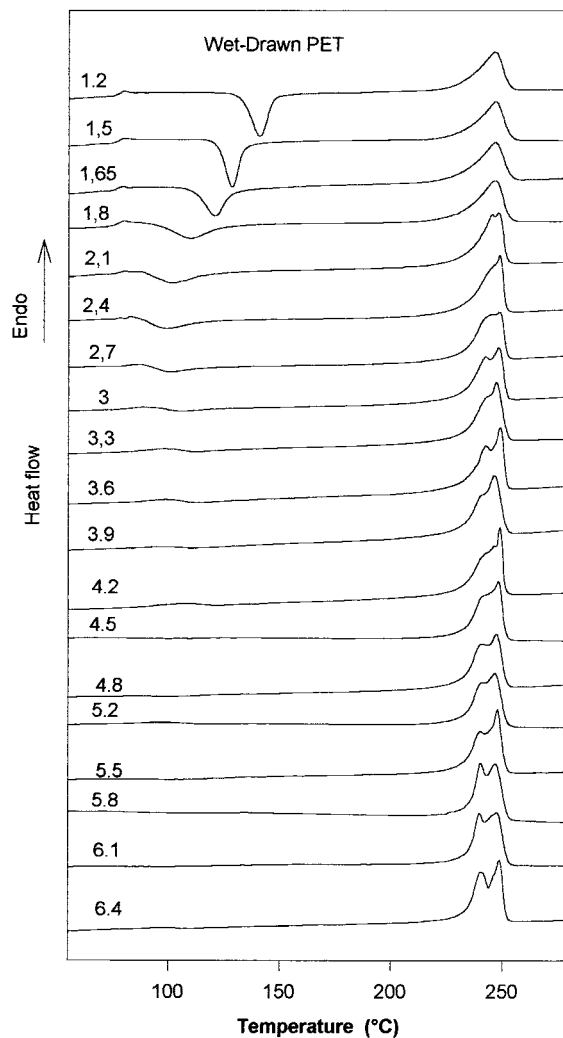


Figure 3 DSC normalized curves for dry samples drawn at various draw ratio (indicated on the figure). The curves are shifted on the heat flow axis for legibility.

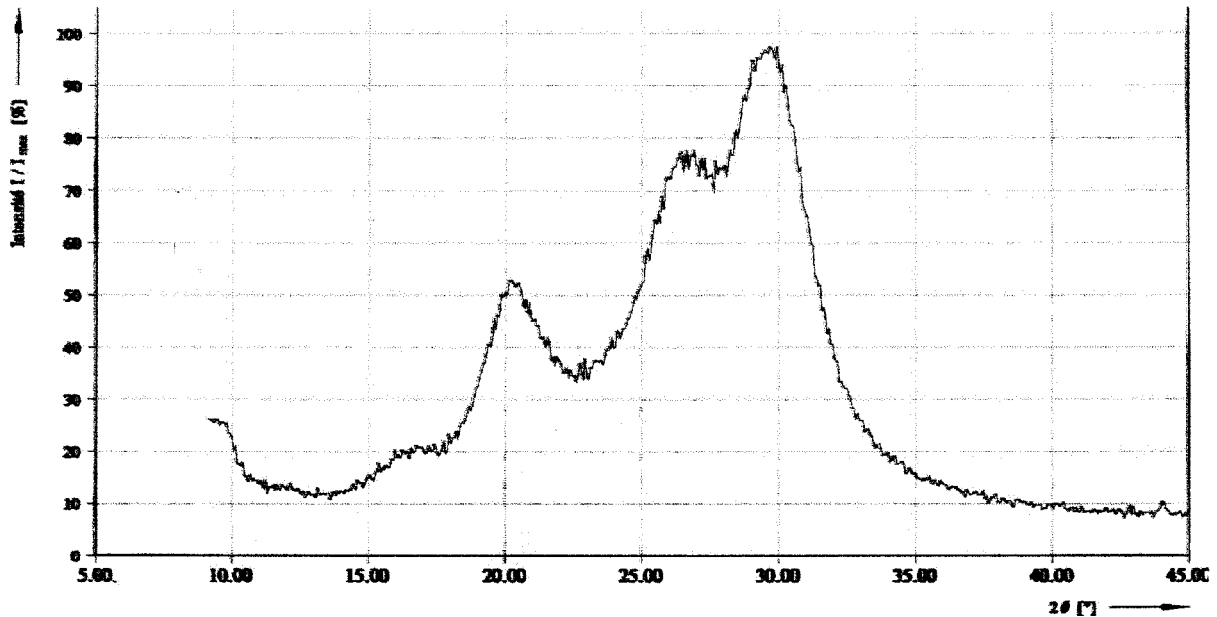


Figure 4 WAXS analysis: Scattered intensity (in %) versus 2θ (in degrees).

drawn PET. The shape of the peak of fusion is also modified, for dry-drawn samples, it is more asymmetric, while for the wet-drawn samples, it appears as due to the superimposition of two fusion reactions.

For $\lambda > 4$, the glass transition is no more observable (for this heating rate) and the samples do not crystallize. For wet-drawn samples, the melting, now clearly composed of two peaks, shows the fusion of two different species of crystallites.

X-Ray Diffraction

Figure 4 shows the normalized intensity (I/I_{\max} in %) versus 2θ (in degrees) for a wet-drawn sam-

ple with $\lambda = 4.8$. The XRD patterns, quasi-similar for the different studied samples, show the three main diffraction peaks at 2θ equal to 20, 27, and 30°, corresponding respectively to the planes (010), ($\bar{1}10$), and (100) of the triclinic lattice structure of crystalline PET.¹⁵ The intensities of the maximum of the three peaks are reported in Table I. In principle, it is possible to determine the degree of crystallinity from the relative areas under the crystalline peaks and the amorphous hump. Practically, it is difficult to resolve the curve into areas due to each phase. Nevertheless, an approximate degree of crystallinity, called X'_c and reported in Table I, can be obtained by a simple construction.¹⁶

Table I WAXS Data

λ	I (010) (Arbitrary Unit)	I ($\bar{1}10$) (Arbitrary Unit)	I (100) (Arbitrary Unit)	X'_c (%)	X_c (%)
Wet-drawn $\lambda < \lambda_{c1}$	NO ^a	NO	NO	0	0
Wet-drawn $\lambda = 3.3$	106	201	177	35	28
Wet-drawn $\lambda = 4.2$	120	224	238	40	36
Wet-drawn $\lambda = 4.8$	169	274	338	43	36
Wet-drawn $\lambda = 6.4$	177	261	334	47	37
Dry-drawn $\lambda < \lambda_{c1}$	NO	NO	NO	0	0
Dry-drawn $\lambda = 3.3$	115	NO	288	38	24
Dry-drawn $\lambda = 4.8$	172	295	374	41	36

Degrees of crystallinity X'_c obtained from WAXS and X_c obtained from DSC analysis.

^a NO indicates "not observable."

DISCUSSION

Dry-Drawn Samples

In regards to the X-ray patterns the samples must be considered as amorphous for the lowest values of the draw ratio ($\lambda < \lambda_{c1}$). The patterns do not exhibit any peak characteristic of a crystalline phase. However, into this drawing zone, the birefringence increases linearly with λ , revealing a gradual growth of the macromolecular orientation, the polymeric chain axis becoming parallel to the draw direction. These linear variations were also observed by Rietsch¹⁴ in this range of λ values. The jump of the birefringence observed at λ_{c1} was already and clearly attributed to the emergence of a strain-induced crystallized structure called the SIC phase, which grows to the detriment of the amorphous phase^{11,12} when λ increases. In a recent work,¹² we have clearly shown by the pole figure and DSC analysis that for the largest deformation ratio $\lambda > \lambda_{c2}$, there is an alignment of the crystalline structure with the draw direction without modification of the degree of crystallization. This is confirmed by the weak increase of the approximate degree of crystallinity X'_c computed from X-ray measurements. The birefringence of the material is related to its degree of crystallinity (X_c) from the following relationship¹³:

$$\Delta n = (1 - X_c)f_a\Delta n_a + X_cf_c\Delta n_c \quad (1)$$

where f_i and Δn_i are, respectively, the orientation factors and the birefringence of a , the amorphous phase, and c , the crystalline phase. However, depending on the authors, the values of Δn_c proposed in the literature lie between 0.212¹⁷ and 0.290¹⁸; and for the amorphous phase, we find Δn_a between 0.200¹⁹ and 0.275.²⁰ In regard to uncertainties on Δn_c and Δn_a , it seems difficult to correlate the birefringence measurements with the degree of crystallization. Thus, at this stage of the discussion, we can only conclude that orientation of both the amorphous and the crystalline phases have reached its maximum for $\lambda > \lambda_{c2}$ because the maximum birefringence that we obtain is very close to the values of Δn_a and Δn_c .

Wet-Drawn Samples

The general scheme observed on the dry-drawn sample remains available, as follows: (1) orientation of the amorphous phase ($\lambda < \lambda'_{c1}$); (2) ap-

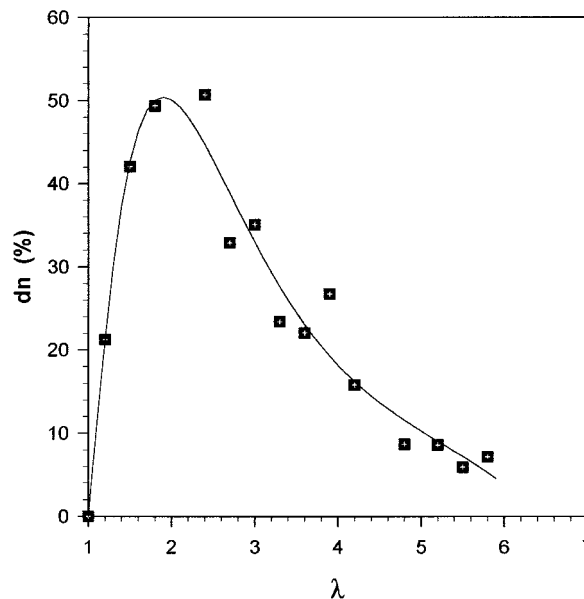


Figure 5 Variations of the relative birefringence between wet-drawn and dry-drawn samples versus λ .

pearance of the SIC phase ($\lambda'_{c1} < \lambda < \lambda_{c2}$); and (3) orientation of the SIC phase ($\lambda > \lambda_{c2}$). However, the birefringence shows the following slight differences between the dry- and the wet-drawn samples: (1) for a given draw ratio, the values $\Delta n(\text{wet})$ are lower than the values of the dry-drawn samples, and (2) there is a weak shift toward higher values for λ_{c1} .

The shift observed for λ_{c1} can be explained by the presence of plasticizer, in this case, the sorbed water molecules. Increasing the average distance between the polymeric chains, they decrease the average intermolecular energies and then make the molecular movements easier. As a consequence, the degree of orientation required to observe the growth of the SIC phase is reached for a higher draw ratio.

It is interesting to observe the relative variation of the birefringence defined by the adimensional number: $dn = [\Delta n(\text{dry}) - \Delta n(\text{wet})] / \Delta n(\text{dry})$. The decrease and the vanishing observed in Figure 5 for dn when $\lambda > 2$ show that the two series of samples exhibit the same optical anisotropy at large deformations. On the other hand, the values of dn are maxima around the first critical value λ_{c1} . We have shown in Figure 1 that the appearance of a SIC phase leads to an important increase of the birefringence. In the drawing zone $[\lambda_{c1}, \lambda'_{c1}]$, the dry-drawn samples are semicrystalline, while the wet-drawn samples are still wholly amorphous, and, as a conse-

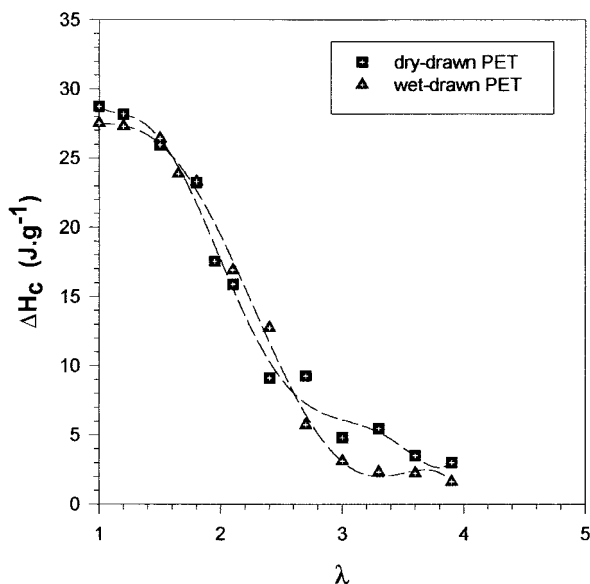


Figure 6 Variations of the enthalpy of the cold crystallization peak versus draw ratio. Lines are drawn as guides for the eyes.

quence, had a lower birefringence. The maxima of the relative birefringence dn is due to the difference of structure between the two series of samples. This is in the range of deformations for which the SIC phase appears; that presence of water molecules during drawing leads to the more important change in optical anisotropy of the resulting film.

Figures 6 and 7, which display the enthalpies of cold crystallization and fusion versus λ , do not show significant differences between dry-drawn and wet-drawn samples. Firstly, we have to consider that Figure 6 characterizes the ability to crystallize for the remaining amorphous phase. So the gradual orientation of the amorphous phase associated with the shift towards lower temperature (see Fig. 8) of the crystallization peak implies the slight decrease of ΔH_c for $\lambda < \lambda_{c1}$.²¹ The appearance of the SIC phase leads to the vanishing of the thermal crystallization of the amorphous phase. This thermal crystallization is spherulitic when no SIC phase exists (for $\lambda < \lambda_{c1}$) and occurs by growth of the SIC phase for $\lambda_{c1} < \lambda < \lambda_{c2}$.²² On the other hand, the value of the enthalpy of fusion is directly related to the degree of crystallinity X_c before DSC scans, which can be estimated from the following equation:

$$X_c = \frac{\Delta H_c^0 - \Delta H_c(T_c^0)}{\Delta H_c^0} \cdot \frac{\Delta H_f}{\Delta H_f^0} \quad (2)$$

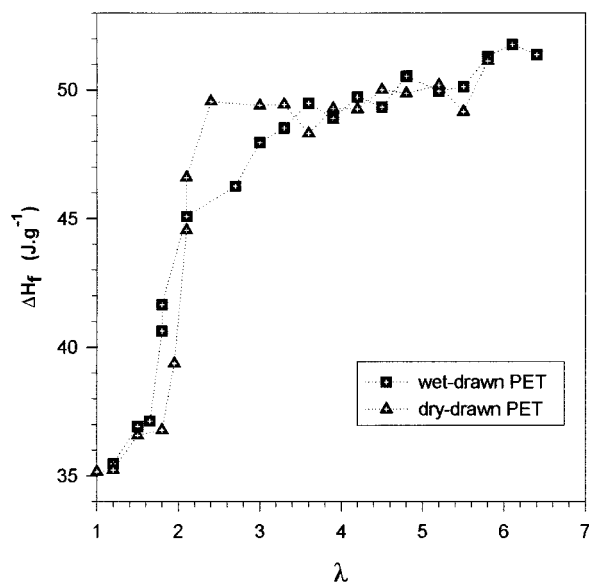


Figure 7 Variations of the enthalpy of fusion versus draw ratio. Lines are drawn as guides for the eye.

in which ΔH_f is the enthalpy of fusion of a sample and ΔH_f^0 is the calculated enthalpy of fusion of wholly crystalline PET ($\Delta H_f^0 = 140 \text{ J g}^{-1}$ ²³), ΔH_c^0 is the enthalpy of crystallization of an undrawn and wholly amorphous sample, $\Delta H_c(T_c^0)$ is the calculated enthalpy of crystallization of the drawn sample bring to the temperature of crys-

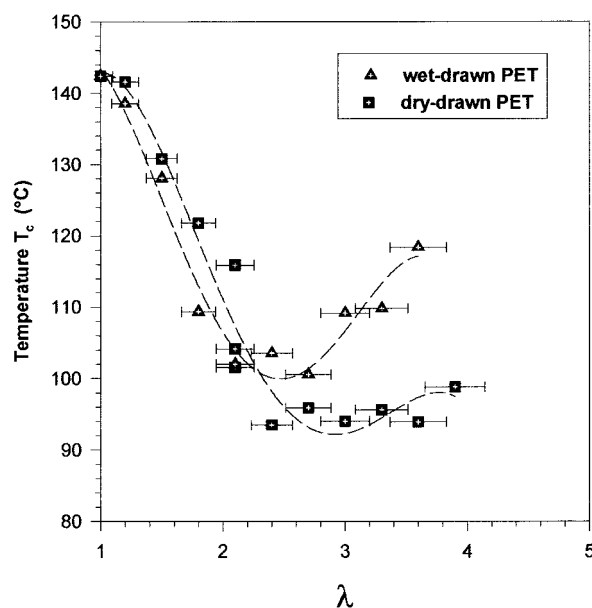


Figure 8 Variations of the temperature T_c (minimum of the thermal crystallization peak) versus draw ratio. Lines are drawn as guides for the eyes.

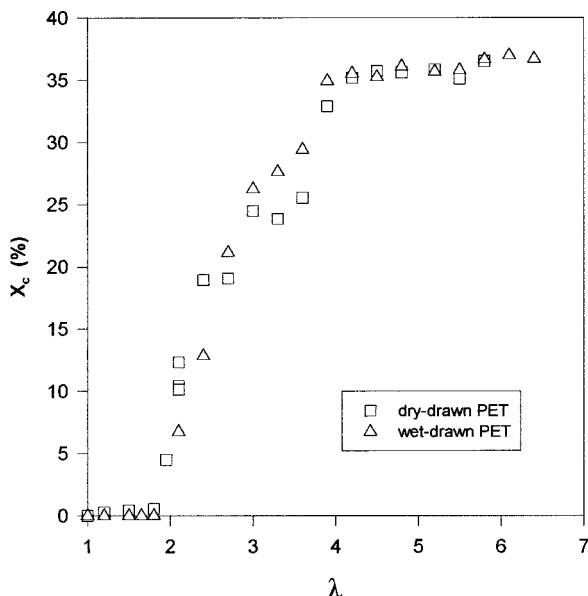


Figure 9 DSC degree of crystallinity versus draw ratio.

tallization of an undrawn sample T_c^0 . This enthalpy $\Delta H_c(T_c^0)$ is determined by the following relation:

$$\Delta H_c(T_c^0) = \Delta H_c(T_c) + \Delta C_p[T_c^0 - T_c] \quad (3)$$

where $\Delta H_c(T_c)$ is the enthalpy of crystallization measured at T_c , ΔC_p is the variation of the thermal capacity at the glass transition for each sample. By this way, only the decrease of the enthalpy due to the diminution of the quantity of crystallites created during the DSC scans is taken into account. From the values of ΔH_f , ΔH_c , and T_c determined in this work (Figs. 6–8), we can estimate the degree X_c of crystallinity reached after a drawing period for dry-drawn and wet-drawn samples (Fig. 9). This degree of crystallinity X_c is also reported in Table I and is in good agreement with X_c' obtained from WAXS analysis. The same three domains are also observable for the two series of samples in Figure 9, as follows: (1) X_c closed to 0 up to $\lambda = \lambda_{c1}$; (2) X_c increases to reach for λ_{c2} 36%; (3) for $\lambda > \lambda_{c2}$, X_c is constant (the cold crystallization enthalpy vanishes, and the melting enthalpy has reached its maximum). Thus, this result confirms that the maximum of SIC phase is obtained for $\lambda \cong \lambda_{c2}$. The main conclusion that we are able to do from these results is that the presence of water molecules during the drawing period does not modify the critical draw ratio at which the degree of crystalliza-

tion has reached its maximum and the percentage of the amorphous phase which crystallizes.

Nevertheless, if the variations of the enthalpy of crystallization and fusion are practically the same for a given λ value; for both dry and wet drawn samples, the value of the temperature at which the crystallization occurs, appears more sensitive to the presence of water during drawing (Fig. 8). This is in the range $\lambda_{c1} < \lambda < \lambda_{c2}$ that differences in the values of T_c are significant. In this range of draw ratio, T_c remains practically constant for the dry-drawn sample ($T_c = 95^\circ\text{C}$), while for the wet-drawn sample, the value of T_c increases as the draw ratio increases to reach 118°C for λ_{c2} . Thermal cold crystallization is known to be sensitive to the existence of a preorientation of the molecular chains,^{21,23} which is a factor contributing to the decrease of the thermal crystallization temperature. Therefore, T_c values are higher for wet-drawn samples than for dry-drawn samples, showing that the amount of oriented molecular species in the remaining amorphous phase of a wet-drawn sample is lower than in dry-drawn sample.

If water molecules can modify orientation of the remaining amorphous phase during drawing without changing the degree of crystallization, we have to investigate the nature of this crystallization. The melting temperature can be linked to the size of the crystallites by the Thomson–Gibbs relationship, as follows:

$$T_f = T_f^0 \left[1 - \frac{1}{\rho_c \cdot \Delta H_f^0} \left(\frac{2\sigma_e}{e} + \frac{4\sigma}{a} \right) \right] \quad (4)$$

where T_f^0 is the melting of the infinite large crystal ($T_f^0 = 280^\circ\text{C}$ ²³), ρ_c is the density of the crystal ($\rho_c = 1.455 \text{ g cm}^{-3}$ ²³), σ_e and σ are the extremities and the lateral surface-free energies ($\sigma_e = 27 \cdot 10^{-7} \text{ J cm}^{-2}$ and $\sigma = 5.75 \cdot 10^{-7} \text{ J cm}^{-2}$ ^{24,25}). In the general case of thermal crystallization, e is the lamellar thickness of the spherulite, and a is the lateral size. For the spherulitic crystallization, a is larger than e , and the term $4\sigma/a$ is negligible. In the case of strain-induced crystallization we can suppose, in a first approach, that the different crystal dimensions are on the same order and introduce a characteristic crystal dimension l with $e \approx a \approx l$. So, equation (4) can be rewritten as

$$l = \frac{2\sigma_e + 4\sigma}{\rho_c \cdot \Delta H_f^0} \cdot \frac{T_f^0}{T_f^0 - T_f} \quad (5)$$

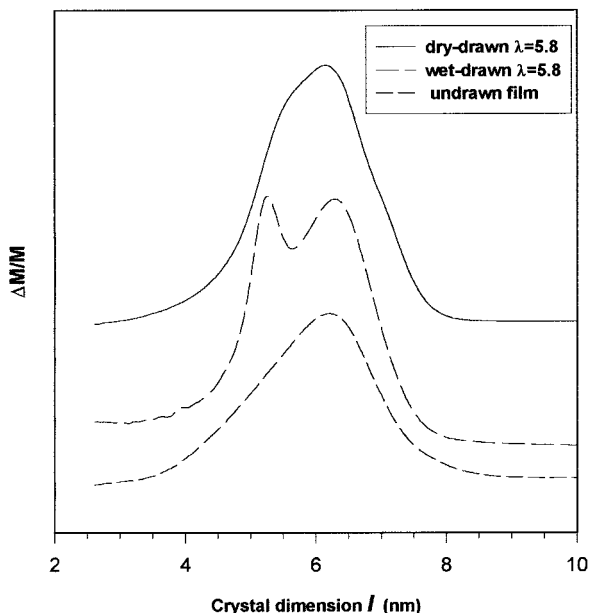


Figure 10 Evolution of crystal size distribution for three PET films, the undrawn, wet-drawn and dry-drawn samples ($\lambda = 5.8$).

From this expression and for a given polymer, it follows that higher the crystalline length l , the higher the fusion temperature. The DSC traces give the evolution of the heat flow ΔQ required to melt a quantity ΔM of the crystalline phase at temperature T . From these curves, the distribution of the weight fraction $\Delta M/M$ versus the crystal dimension l is calculated. M is the weight of the crystalline phase proportional to the total heat flow Q required to melt all the crystallites in the polymer. Figure 10 shows the evolution of $\Delta M/M$ versus l for undrawn, dry, and wet-drawn samples ($\lambda = 5.8$). The comparison of the three curves immediately shows that the wet-drawn sample admits two families of 5.2 and 6.3 nm crystal size. The proportion of thick crystallites is larger than the thin ones. This phenomenon is observed for a wet-drawn samples as soon as the draw ration is equal to λ_{c1} . For the undrawn and dry-drawn samples, only a family of 6.2 nm crystal size is observed. We can suppose that the presence of water molecules have impeded the crystal growth and leads to the appearance of crystallites of smaller sizes. From all these results, we may now propose a complete scenario of the different events, which occur during the drawing period for a wet sample. Up to λ_{c1} , water molecules act as plasticizers, and for a given draw ratio, re-

stricts the molecular orientation [Fig. 11(A)]. For $\lambda_{c1} < \lambda < \lambda_{c2}$, the SIC phase occurs, and the water molecules are excluded from this ordered phase inside the remaining amorphous phase (it is now well established that no water molecules can be trapped inside the crystallites). Some of the water molecules can be blocked near crystallites or between two crystallites and impeded the growth of a part of the crystalline phase. These smallest crystallites are at the origin of the lower fusion peak. Consequently, this increases the relative concentration of water in the amorphous phase. A simple calculation based on a two phase model and for our X_c values allows to determine that the content of water, which was of the order of 1 water molecule per 13 PET monomer units for the amorphous material with $rh = 76\%$ (undrawn and wet samples), would become of 1.6 water molecule per 13 PET monomer units of the remaining amorphous phase (wet-drawn samples). In this range of drawing ratio, the amount of water molecules trapped in the amorphous phase during drawing can undergo beyond the equilibrium limit value reached during a standard absorption measurement (1.3 water molecule per 13 PET monomer). Thus, in this range of deformation, water molecules do not act as classical plasticizers, but impedes the orientation of the amorphous phase by increasing the steric constraints or which is equivalent, and by increasing the size of the water clusters inside the amorphous phase or which is also equivalent, by increasing the mean distance between the main polymeric chains [Fig. 11(b)]. Keeping in mind that dry- and wet-drawn samples exhibit for $\lambda = \lambda_{c2}$, the same maximum degree of crystallinity, the birefringence differences observed can be explained from modifications in the values of the amorphous phase orientation factor (f_a), which occurs in relationship (1). In a first approximation, the values for the other parameters can be supposed equal for dry- and wet-drawn samples. At large deformation, $\lambda = \lambda_{c2}$, the water clusters practically disappear [Fig. 11(c)], and for $\lambda > \lambda_{c2}$, the deformation becomes so large as to allow the orientation of the crystal.

CONCLUSIONS

In this work, the presence of water molecules during drawing of PET films was investigated.

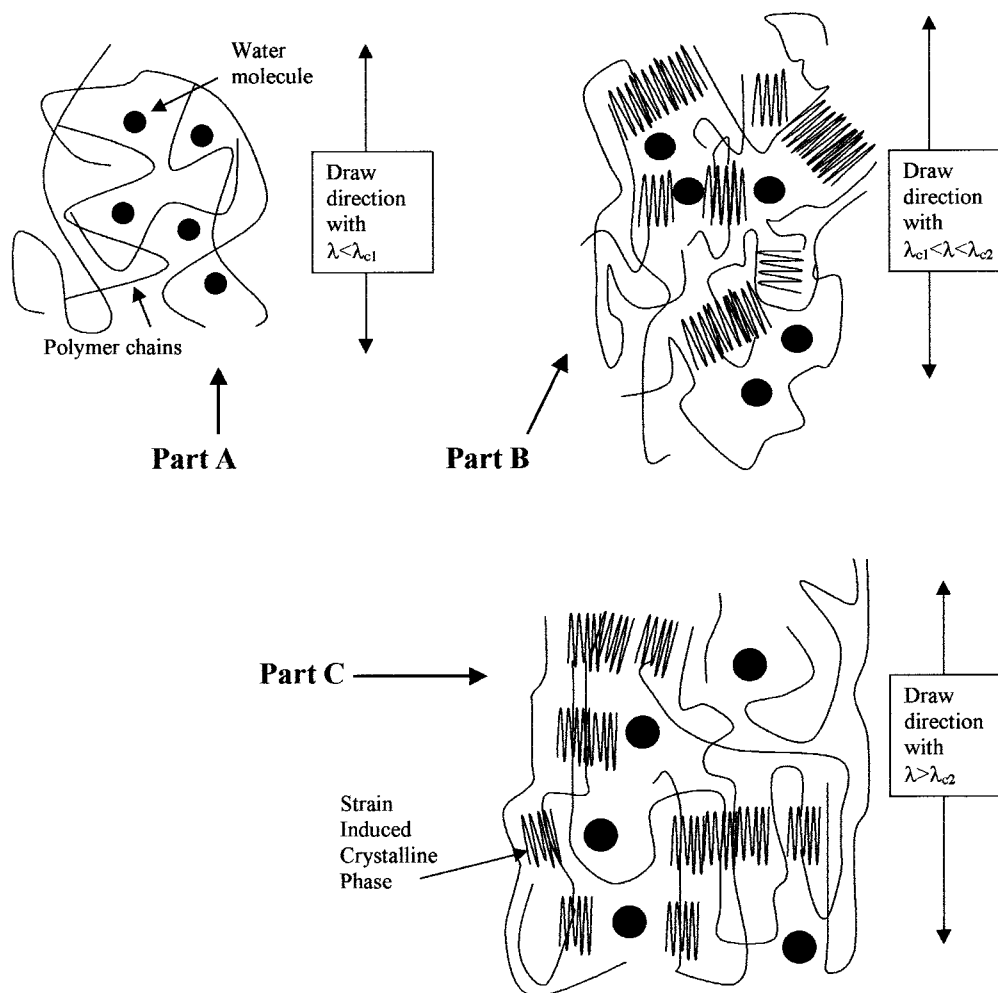


Figure 11 Schematic representation of the role of water molecules during the drawing: (a) for $\lambda < \lambda_{c1}$; (b) for $\lambda_{c1} < \lambda < \lambda_{c2}$; (c) for $\lambda > \lambda_{c2}$.

For a low draw ratio, the water molecules play their traditional plasticizer effects. For a draw ratio included between two critical values which respectively correspond to the emergence of the SIC phase and to the maximum degree of crystallinity (λ_{c1} , λ_{c2}), weakly sensitive to the presence of water molecules, the orientation of the remaining amorphous phase is also affected. In the later case, water molecules act as blocking molecules that impede the orientation of the amorphous phase. At a large draw ratio, the effects of the water molecules on the orientation of the amorphous phase decrease and vanish for approximately a draw ratio of 6. Water molecules had also an influence on the strain-induced crystallization by modifying the crystallites sizes distribution. Some of the crystallites had a smaller size due to water molecules, which impede the crystal growth.

The authors are indebted to A. Dahoun and A. Thil, of the University of Metz, for performing the X-ray determination.

REFERENCES

1. Fukada, M.; Kawai, H. *Polymer* 1990, 31, 295.
2. Jabarin, S. A.; Lofgren, E. A. *Polym Eng Sci* 1983, 26, 620.
3. Langevin, D.; Grenet, J.; Saiter, J. M. *Eur Polym J* 1994, 30, 339.
4. Byershtein, V. A.; Yegorova, L. M.; Yegorov, V. M.; Sinani, A. B. *Polym Sci USSR* 1989, 31, 2719.
5. Saiter, J. M.; Langevin, D.; Lebaudy, P.; Grenet, J. *J Non-Cryst Solids* 1994, 172–174, 640.
6. Slee, J. A.; Orchard, G. A. J.; Bower, D. I.; Ward, I. M. *J Polym Sci, Polym Phys Ed* 1989, 27, 71.
7. Orchard, G. A. J.; Pspiby, P.; Ward, I. M. *J Polym Sci, Polym Phys Ed* 1990, 28, 603.

8. Jabarin, S. A. *J Appl Polym Sci* 1987, 34, 103.
9. Toda, T.; Yoshida, H.; Fukunishi, K. *Polymer* 1995, 36, 699.
10. Zimmerman, H.; Nguyen, T. K. *Polym Eng Sci* 1980, 20, 680.
11. Dargent, E.; Grenet, J.; Auvray, X. *J Therm Anal* 1994, 41, 1409.
12. Dargent, E.; Grenet, J.; Dahoun, A. *Polym Eng and Sci* 1997, 37, 1853.
13. Hay, I. L. *Methods of Experimental Physics*, Vol. 16, Part C; Fava, R. A., Ed.; Academic Press: New York, 1980; p 163.
14. Rietsch, F. *Eur Polym J* 1990, 10, 1077.
15. Daubeny, R. de P.; Bunn, C. W.; Brown, C. J. *J Proc R Soc London A* 1954, 226, 531.
16. Young, R. J. *Introduction to Polymers*; Chapman and Hall: London, UK, 1983, p. 174.
17. Konda, A.; Nose, K.; Ishikawa, H. *J Polym Sci A2* 1976, 14, 1495.
18. Gupta, V. B.; Kumar, S. *J Polym Sci, Polym Phys Ed* 1979, 17, 1307.
19. Devries, A. J.; Bonnebat, C.; Beautemps, J. *J Polym Sci, Polym Symp* 1977, 58, 109.
20. Dumbleton, J. H. *J Polym Sci A2* 1968, 6, 795.
21. Hagege, R.; Mamy, C.; Thiroine, C. *Makromol Chem* 1978, 179, 1069.
22. Dargent, E.; Denis, A.; Galland, C.; Grenet, J. *J Therm Anal* 1996, 46, 377.
23. Wunderlich, B. *Macromolecular Physics*, Vol. 3; Academic Press: New York, 1980.
24. Elenga, R. G.; Seguela, R.; Rietsch, F. *Polymer* 1991, 32, 1975.
25. Baranov, V. G.; Kenarov, A. V.; Volkov, T. I. *J Polym Sci, Polym Symp* 1970, 30, 271.